

# Plasmon-assisted mode selection lasing in a lanthanide-based microcavity

Lei Guo,<sup>a</sup> Min Ji,<sup>a</sup> Bowen Kang,<sup>a</sup> Min Zhang,<sup>a</sup> Xin Xie,<sup>a</sup> Zihao Wu,<sup>a</sup> Huan Chen,<sup>a,\*</sup> Volker Deckert,<sup>b</sup> and Zhenglong Zhang<sup>a,\*</sup>

<sup>a</sup>Shaanxi Normal University, School of Physics and Information Technology, Xi'an, China

<sup>b</sup>Friedrich-Schiller University, Leibniz Institute of Photonic Technology, Jena, Germany

**Abstract.** Lanthanide-based microlasers have attracted considerable attention owing to their large anti-Stokes shifts, multiple emission bands, and narrow linewidths. Various applications of microlasers, such as optical communication, optical storage, and polarization imaging, require selecting the appropriate laser polarization mode and remote control of the laser properties. Here, we propose a unique plasmon-assisted method for the mode selection and remote control of microlasing using a lanthanide-based microcavity coupled with surface plasmon polaritons (SPPs) that propagate on a silver microplate. With this method, the transverse electrical (TE) mode of microlasers can be easily separated from the transverse magnetic (TM) mode. Because the SPPs excited on the silver microplate only support TM mode propagation, the reserved TE mode is resonance-enhanced in the microcavity and amplified by the local electromagnetic field. Meanwhile, lasing-mode splitting can be observed under the near-field excitation of SPPs due to the coherent coupling between the microcavity and mirror microcavity modes. Benefiting from the long-distance propagation characteristics of tens of micrometers of SPPs on a silver microplate, remote excitation and control of upconversion microlasing can also be realized. These plasmon-assisted polarization mode-optional and remote-controllable upconversion microlasers have promising prospects in on-chip optoelectronic devices, encrypted optical information transmission, and high-precision sensors.

Keywords: lanthanide-based microlaser; surface plasmon polaritons; polarization mode selection.

Received Dec. 31, 2023; revised manuscript received Mar. 11, 2024; accepted for publication Apr. 7, 2024; published online May 8, 2024.

© The Authors. Published by SPIE and CLP under a Creative Commons Attribution 4.0 International License. Distribution or reproduction of this work in whole or in part requires full attribution of the original publication, including its DOI.

[DOI: [10.1117/1.AP.6.3.035001](https://doi.org/10.1117/1.AP.6.3.035001)]

## 1 Introduction

Microcavity lasing has many excellent properties, such as a small mode volume, high quality factor ( $Q$ ), high sensitivity, effortless manipulation, and good monochromaticity, which can be applied in sensing,<sup>1-3</sup> nonlinear optics,<sup>4-6</sup> and cavity optomechanics.<sup>7,8</sup> The superior features of lanthanide-doped upconversion nanoparticles (UCNPs), such as their sharp emission bands, long lifetime, nonblinking and nonbleaching characteristics, and high stability,<sup>9,10</sup> make them an attractive gain medium for the development of upconversion microlasers. Moreover, they have real intermediate energy states as efficient media for the development of multiphoton-excited states.

Lanthanide-based microcavity lasing has attracted considerable attention owing to its large anti-Stokes shifts, multiple emission bands, and narrow linewidths.<sup>11-14</sup> Many advances have been made, such as the effective regulation of laser modes, the realization of low-threshold microlasers, and the achievement of up-converted lasing.<sup>15-19</sup> With the miniaturization of optoelectronic devices, various applications of lanthanide-based microlasers, such as optical communication, optical storage, and polarization imaging, require selecting the appropriate laser polarization mode and controlling the laser properties remotely on-chip. However, controlling the polarization mode of microlasing, a fundamental property of microlasers, both *in situ* and remotely, remains challenging.

Surface plasmon polaritons (SPPs) propagate at the interface between a metal conductor and dielectric in the form of electromagnetic waves<sup>20</sup> and can constrain and manipulate optical

\*Address all correspondence to Huan Chen, [hchen@snnu.edu.cn](mailto:hchen@snnu.edu.cn); Zhenglong Zhang, [zizhang@snnu.edu.cn](mailto:zizhang@snnu.edu.cn)

signals in subwavelength structures over long distances. Because of the limitations of the surface boundary conditions, only the transverse magnetic (TM) polarization mode surface waves of the SPPs can propagate at the metal–air interface. The unique properties of the SPPs provide an effective method for separating and selecting the polarization modes of lanthanide-based microlasers. However, traditional mode selection methods such as reducing cavity size, increasing mode selection structure, and Vernier efficacy-based methods, which adjust the laser mode by reducing the number of modes, cannot effectively select the laser polarization mode, and compared with pure silicon-based devices used for polarization beam splitters,<sup>21</sup> SPP-based devices provide a compact size and a remote-control interface for on-chip applications.<sup>22–24</sup>

In this letter, a simple and effective plasmon-assisted mode selection method for a lanthanide-based whispering gallery mode (WGM) microlaser is proposed. A plasmon-assisted lanthanide-based microcavity composed of a silver microplate is used as a substrate, on which a UCNP-coated SiO<sub>2</sub> (SiO<sub>2</sub>@UCNPs) microsphere is placed. Compared with lanthanide-based microlasers, the transverse electric (TE) mode lasing of plasmon-assisted lanthanide microlasers can be selectively enhanced by

the enhanced local electric field and long-distance propagation of plasmons. Meanwhile, under the near-field excitation of SPPs, lasing mode splitting can be observed owing to the coherent coupling between the microcavity and mirror microcavity modes. The remote excitation and control of upconversion microlasing can also be achieved by propagating SPPs. The proposed mode-selection method has promising prospects for on-chip optoelectronic devices, encrypted optical information transmission, and high-precision sensors.

## 2 Results and Discussion

In this letter, a plasmon-assisted mode selection lanthanide-based microcavity was realized by placing a single UCNP-coated SiO<sub>2</sub> microsphere on a monocrystalline silver microplate, as illustrated in Fig. 1(a). Using the UCNP-coated SiO<sub>2</sub> microspheres, WGMs could be generated through total internal reflection, facilitating whispering gallery lasing through the fluorescence of the coupled UCNPs. NaYF<sub>4</sub>:20% Yb<sup>3+</sup>/2% Tm<sup>3+</sup> UCNPs with ~11-nm diameter were synthesized using a high-temperature thermal decomposition method,<sup>25,26</sup> as shown in Fig. 1(b) (i) and Fig. S1 in the [Supplementary Material](#).

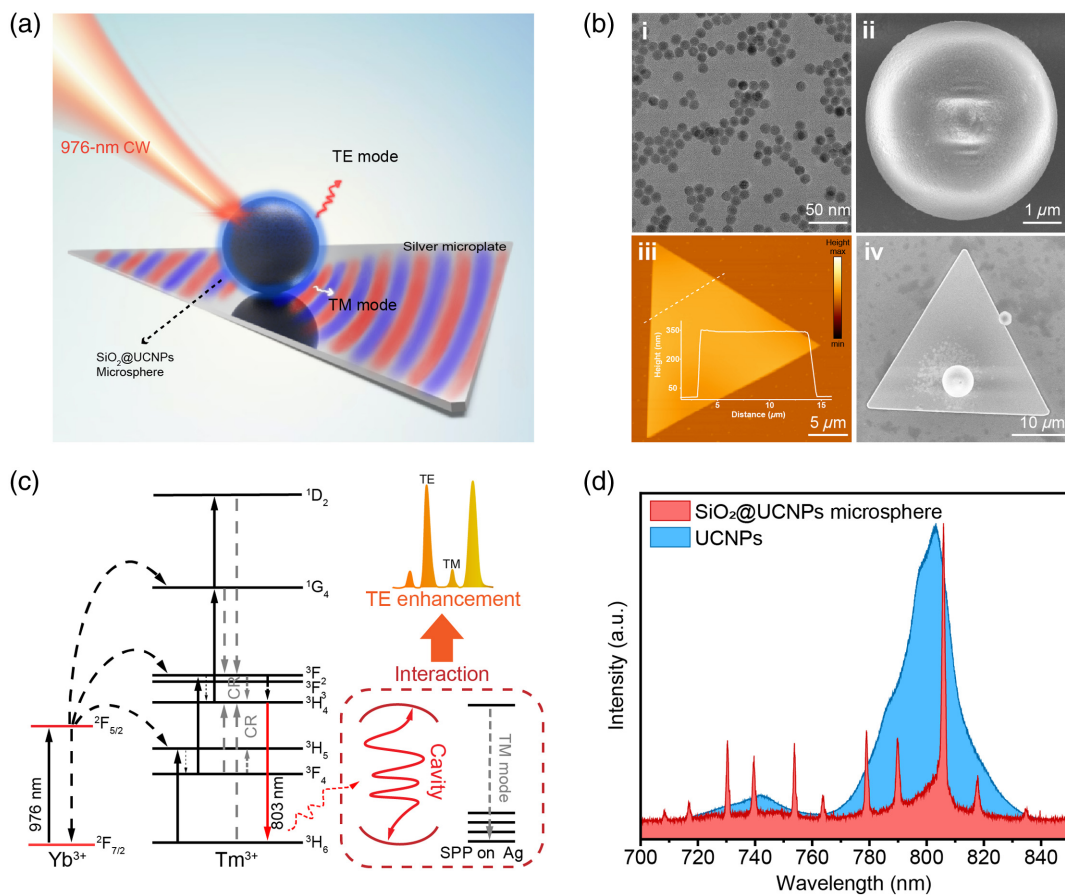


**Fig. 1** (a) Schematic diagram of the plasmon-assisted mode selection lanthanide-based microcavity. (b) Transmission electron microscope image of (i) NaYF<sub>4</sub>:20% Yb<sup>3+</sup>/2% Tm<sup>3+</sup> UCNPs, (ii) scanning electron microscope (SEM) image of SiO<sub>2</sub>@UCNP microsphere, (iii) atomic force microscope image of the silver microplate and its corresponding height profile, and (iv) SEM image of SiO<sub>2</sub>@UCNP microsphere on the silver microplate. (c) Simplified energy-level diagram describing the plasmon-assisted selective enhancement process of the TE mode. (d) Fluorescence emission spectra of UCNPs and a SiO<sub>2</sub>@UCNP microsphere.

To realize upconversion lasing, UCNPs, as gain media, were uniformly coated on the surface of the SiO<sub>2</sub> microsphere using the spin-coating method [Fig. 1(b) (ii)]. The fabricated microcavities maintained a perfectly spherical shape and smooth morphology, which effectively reduced the scattering loss in the optical resonance and spontaneous emission background, thereby guaranteeing high-quality and low-threshold laser operation. A silver microplate was placed under the fabricated microcavity as a carrier to generate propagating SPPs. As shown in Fig. 1(b) (iii), the monocrystalline silver microplates with ~350-nm thickness were prepared by a fast one-step synthesis in a water solution at room temperature, as reported in our previous study.<sup>27,28</sup> These microplates are characterized by their low ohmic loss, long-distance transmission SPPs, SPP distribution, and mode adjustment properties.<sup>29</sup> Subsequently, the micromanipulation technique was used to transfer an individual SiO<sub>2</sub>@UCNP microsphere onto a specific silver microplate, and the microcavity used for plasmon-assisted mode selection was successfully constructed. Figure 1(c) illustrates the physical mechanism of the plasmon-assisted mode-selection microlaser, in which the fluorescence of Tm<sup>3+</sup> resonated in the microcavity, resulting in lasers with two different polarization modes. The TM mode of the laser propagated on the surface of the microplate because the SPPs of the silver microplate could only support TM mode propagation. The reserved TE mode was further resonance-enhanced in the microcavity and amplified by the local electromagnetic field of the plasmons. Therefore, the selective enhancement of TE mode lasing was realized.

First, we investigated the characteristics of upconversion lasing from a single SiO<sub>2</sub>@UCNP microcavity. Figure 1(d) displays the upconversion fluorescence spectra of UCNPs and a SiO<sub>2</sub>@UCNP microcavity with a diameter of 5 μm under the 976-nm continuous-wave laser excitation. The blue curve depicts the fluorescence peak of the UCNPs at 803 nm, corresponding to the upconversion emission from the <sup>3</sup>H<sub>4</sub> to <sup>3</sup>H<sub>6</sub> energy level. When the doping concentration of Tm<sup>3+</sup> increases to 2% with 20% Yb<sup>3+</sup> as the sensitizer, Yb<sup>3+</sup> ion has a large absorption cross section for 976 nm and absorbs photon energy to transfer to Tm<sup>3+</sup> ion (activator), Tm<sup>3+</sup> ion absorbs photon energy to reach different excited states <sup>3</sup>H<sub>5</sub>, <sup>3</sup>F<sub>2,3</sub>, <sup>1</sup>G<sub>4</sub>, and <sup>1</sup>D<sub>2</sub> levels, and a highly excited Tm<sup>3+</sup> ion transfers a fraction of its energy to a neighboring Tm<sup>3+</sup> ion in its ground state,

resulting in two Tm<sup>3+</sup> ions in the same intermediate excited state. The enhanced cross-relaxation of (<sup>1</sup>D<sub>2</sub>, <sup>3</sup>H<sub>6</sub> → <sup>3</sup>F<sub>2</sub>, <sup>3</sup>H<sub>4</sub>), (<sup>1</sup>G<sub>4</sub>, <sup>3</sup>F<sub>4</sub> → <sup>3</sup>F<sub>2,3</sub>, <sup>3</sup>H<sub>4</sub>) and (<sup>3</sup>F<sub>2,3</sub>, <sup>3</sup>F<sub>4</sub> → <sup>3</sup>H<sub>4</sub>, <sup>3</sup>H<sub>5</sub>) will facilitate population inversion at the intermediate state of <sup>3</sup>H<sub>4</sub> and amplify the corresponding 803-nm emission for upconversion lasing.<sup>13</sup> The red curve depicts the efficient upconversion lasing of the TM and TE multimode mixtures produced by the UCNPs coupled to the microcavity. The lasing corresponding to the fluorescence emission peak at 803 nm of the UCNPs shows a narrow linewidth and high efficiency, which demonstrates the excellent laser emission characteristics of the constructed microcavity.

The emission spectra were monitored at various excitation powers to confirm the generation of microlasing and characterize its behavior. In Fig. 2(a), the red and blue point plots represent the pumping power-dependent plots for the integrated emission intensity and spectral linewidth of the 802-nm lasing peak, respectively. The emission intensity is calculated by integrating the lasing peak, which exhibits a sharply increasing slope as the laser power increases, corresponding to a lasing threshold; the spectral linewidth narrows sharply at the lasing threshold, which proves the generation of a low-threshold and narrow-linewidth microlaser. To investigate the polarization anisotropy of the microlaser and distinguish between the TM and TE modes, the fluorescence emission spectra of the microlaser were collected at different polarization angles. In Fig. 2(b), the red triangles and blue spheres denote the polarization-dependent intensities of the 788- and 802-nm lasing, respectively, representing linear polarization-dependent emission vertically and horizontally. The polarization at 788 nm corresponds to the collected polarization angle of 90 deg, which corresponds to TM mode lasing. The 802-nm lasing corresponds to TE mode lasing owing to the lasing action, exhibiting strong polarization with the dominant optical feedback path perpendicular to the equatorial plane of the microcavity. The *Q* factor and full width at half-maximum (FWHM) of the 788- and 802-nm lasing were investigated while altering the polarization angle and were also found to be orthogonal (Fig. S2 in the [Supplementary Material](#)). It should be noted that the FWHM of the lasing lines 802 nm could reach a narrowness of 0.35 nm for these SiO<sub>2</sub>@UCNP microspheres, while *Q* factors on the order of 2500 were estimated based on these precise FWHM measurements.

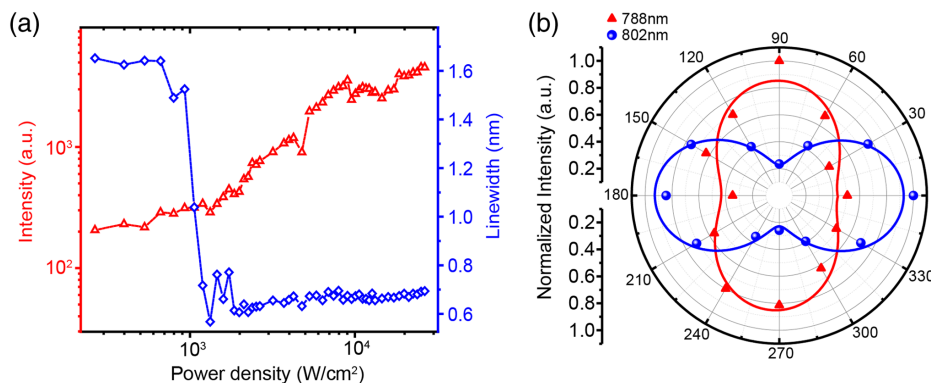


**Fig. 2** (a) Pumping power-dependent plots of emission intensities and spectral linewidth narrowing of 802-nm lasing on the glass substrate exhibiting upconversion lasing emissions. (b) Polarization investigation of the 788- and 802-nm lasing lines using a polar plot of the intensities; the fitting curves were drawn by a cosine-square function.

Based on the high-efficiency narrow-linewidth upconversion lasing, a single lanthanide-based microcavity was placed on a single silver microplate using a micromanipulation transfer technique to realize plasmon-assisted mode selection. As shown in the upper left of Fig. 3(a), a lanthanide-based microcavity was successfully transferred onto a silver microplate. The fluorescence emission spectra of the  $\text{SiO}_2\text{@UCNP}$  microspheres were measured before and after transfer onto a silver microplate. The TE mode exhibited significant enhancement on the silver microplate compared with that on glass, as shown in Fig. 3(a). By contrast, no noticeable intensity changes were observed for TM mode lasing. The microcavity, combined with the silver microplate, exhibited a polarization beam-splitting effect, and the TE mode could be selected and enhanced. We further verified the validity of the plasmon-assisted mode selection by adding polarizers to the collection optical path and setting the polarization parallel to the microsphere radial to 0 deg. Polarization lasing perpendicular to the radial polarization of the microsphere was mainly observed when the polarization of the collection was 90 deg, corresponding to TM mode lasing. As shown in Fig. 3(b), the TM mode lasing intensity was slightly stronger than that of the full-space collection in Fig. 3(a), and the TE mode lasing intensity was slightly weaker. The TM polarization collection experiment weakened the function of plasmon mode selection but proved the effectiveness of plasmon-assisted TE mode selection. Furthermore, the slight blueshift observed in the lasing compared with the simulation

results could be attributed to the change of distribution of UCNP on the surface of the microsphere when the microcavity was transferred onto the silver microplate using the optical fiber tip and the change of the surrounding environment of the microcavity during the micromanipulation process.

To reveal the mechanism of the plasmon-assisted TE mode selection, an electromagnetic field analysis of the silver microplate-coupled microcavity was performed. A point dipole source with a wavelength of 800 nm was used to represent the fluorescence emission of the UCNP, which was placed at the position of the strongest electric field in the silver microplate and microcavity coupling system for subsequent simulation. We first simulated the far-field radiation spectra of the dipole source in the microcavity and silver microplate-coupled microcavity, as shown in Fig. 3(c). The black line represents the far-field radiation spectrum of the dipole source in the microcavity, and the intensities of each pair of the TE and TM modes are equal. The red line represents the far-field radiation of the dipole source in the silver microplate-coupled microcavity. The overall intensity of the TE and TM modes was enhanced relative to the dipole source in the microcavity, whereas the TM mode intensity was weaker than the TE mode intensity. The results showed the same TE mode selection effect as that in the experiment. We further simulated the charge distribution on the silver microplate surface using a microcavity-coupled silver microplate system. Because the fluorescence of UCNP has no polarization characteristics, the luminescence of UCNP was simulated using different dipole

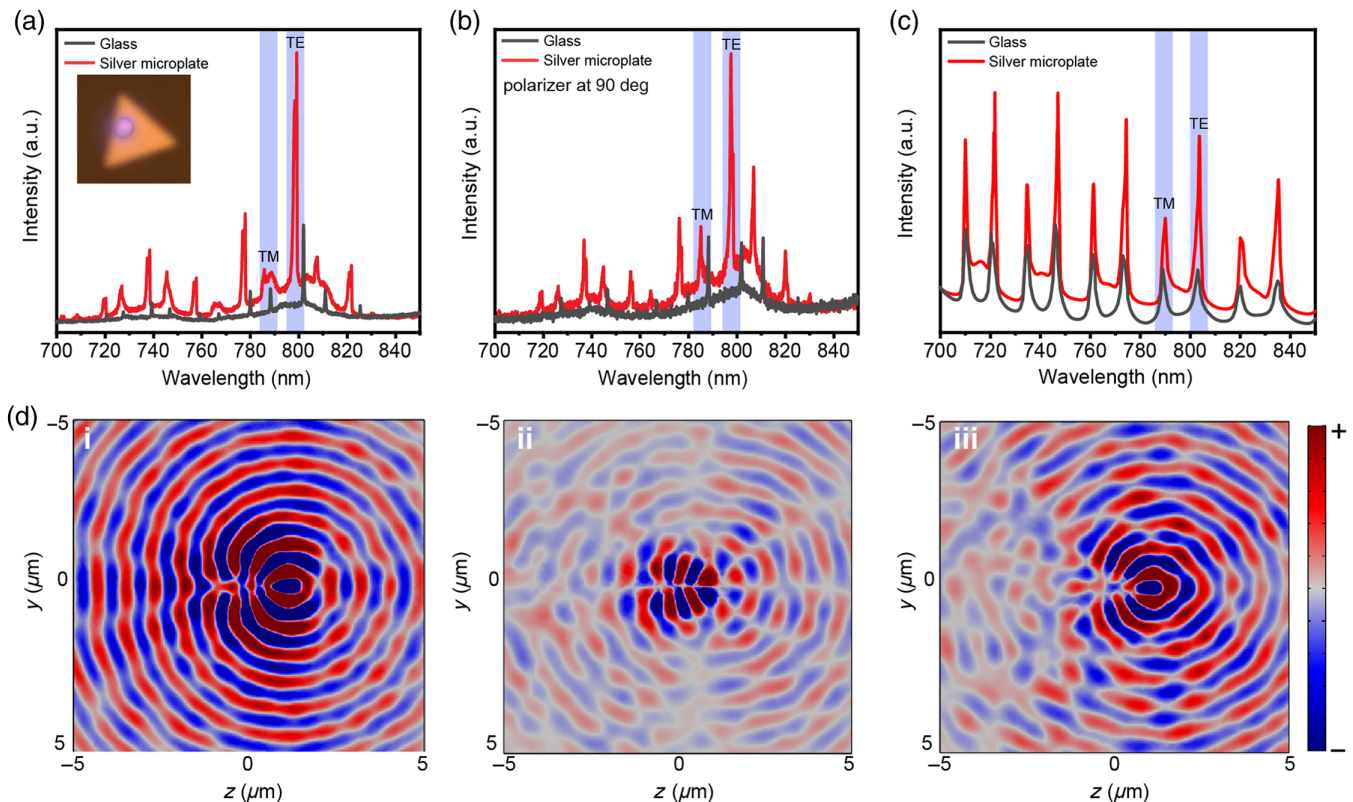


**Fig. 3** (a) Fluorescence emission spectra of  $\text{SiO}_2\text{@UCNP}$  microspheres on the glass substrate and silver microplate. (b) Emission polarization spectra of  $\text{SiO}_2\text{@UCNP}$  microspheres on the glass substrate and silver microplate when the polarizer was at 90 deg. (c) COMSOL-simulated emission spectra corresponding to panel (a). (d) Charge distribution diagram of the silver microplate excited by (i)  $E_x$ , (ii)  $E_y$ , and (iii)  $E_z$  dipole on the microsphere.

electric field orientations. We defined the  $x$  axis along the radial direction of the microsphere, the  $y$  axis perpendicular to the paper surface, and the  $z$  axis horizontally along the tangential direction of the microsphere. As shown in Fig. 3(d) (i), when the  $E_x$  (dipole field oriented in the  $x$  direction) dipole excited the microlaser, the lasing TM mode was transmitted on the silver microplate by the SPPs. When the  $E_y$  dipole excited the microlaser, a significantly weak charge distribution was observed. When the  $E_z$ -stimulated WGM was stimulated, as shown in Fig. 3(d) (iii), a portion of the SPP transmission phenomenon was observed, as the excited electric field  $E_z$  contained components in the direction of the TM, and part of the dipole energy was transmitted by SPPs on the silver microplate. The dipole-TM directional component could also be transmitted as SPPs on a silver microplate, as demonstrated when simulating the charge distribution on a silver microplate with a single dipole placed in the same position without a microcavity (Fig. S7 in the [Supplementary Material](#)). Interestingly, we found that both  $E_x$  and  $E_z$  transmitted SPPs owing to the TM component because the polar coordinates of the dipole electric field orientation and polar coordinates of the silver microplate had a certain angle, so the  $y$  direction of the two polar coordinates was parallel, and the  $x$  and  $z$  directions have a certain angle; consequently, the electric fields in the  $x$  and  $z$  directions include the TM component. However, on the silver microplate,  $E_z$  only transmitted SPPs on the right side, and the left side could not transmit SPPs because of the presence of the microcavity. Because the TM mode of the  $E_z$  excitation microlaser is weak, it is believed that the SPPs generated by  $E_z$  excitation on the silver microplate were caused by the dipole source itself. Therefore, the TM mode lasing on the silver microplate was significantly weakened compared with that of the TE mode. The intensities of the TE and TM modes were compared using the spectral data in Fig. 3(a) and the simulation in Fig. 3(c) for a more intuitive and clear comparison (see Table S1 in the [Supplementary Material](#)). As shown in the table, the intensity ratio between the TE and TM modes on the silver microplate was always larger than that on the glass substrate for both the experiment and simulation. The experimental and simulation results show that the selective enhancement of the TE mode can be achieved using a plasmon-assistant method. On the one hand, the fluorescence emission of UCNPs coupled with a microcavity is amplified by the local electromagnetic field effect of plasmons; on the other hand, the SPPs of silver microplates can support the propagation of TM mode lasing and weaken the intensity of TM mode lasing.

The lasing mode was also split on the silver microplate when investigating plasmon-assisted mode selection. As shown in Fig. 4(a), the TE mode lasing peak at 798 nm splits into two peaks. We represent the modes of these two peaks as modes 1 and 2. Polarization-dependent spectra were collected to distinguish between the two modes. As shown in Fig. 4(b), when the polarization was collected at 0 deg, the right peak was dominant, whereas when collected at 90 deg, the left peak prevailed. The intensities of the split left and right peaks were compared, resulting in a drafted table (see Table S2 in the [Supplementary Material](#)). The intensity ratio of modes 1 and 2 changed from 1.43 at 0 deg to 0.63 at 90 deg, indicating that the polarizations of modes 1 and 2 were orthogonal. Interestingly, the plasmon-assisted microlaser was different from the conventional WGM microlaser when a mirror microcavity was introduced by the silver microplate, and the two microcavity modes were coherently coupled to form two orthogonal modes, as shown in Fig. 4(a), resulting in the phenomenon of modes 1 and 2 splitting.<sup>30</sup> To explain the mechanism by which the microsphere creates a mirror cavity on the silver microplate and splits the lasing peaks, we used a two-sphere system to simulate the electric field distribution profile (see Fig. S13 in the [Supplementary Material](#)). Dipoles with different orientations were placed between the two spheres owing to coupling with the second microsphere once the degenerate mode was split into two different modes. Polarization degeneracy in excitation lifted, and modes 1 and 2 were excited using orthogonal input polarizations. Both modes exhibited a continuous total internal reflection along the periphery of the sphere. Because the input polarizations of the excited modes were orthogonal, the outcoupled radiation preserved this orthogonality.

In addition to inducing lasing mode selection, SPPs propagating over long distances on a silver microplate also present an opportunity for remote manipulation of microlasers. As shown in the bright-field image in Fig. 5(a), the red circle represents the excitation position, and  $\theta$  (in deg) represents the polarization angle of the excitation light. When the edge of a silver microplate is excited by a laser with a suitable polarization angle, the SPPs propagating to the microcavity can be excited by edge-side scattering to provide momentum-matching conditions, and the microlaser can be excited remotely. It is evident from the spectrum that lasing excitation was observed. The lasing reached its peak intensity at an excitation polarization angle of  $\sim 100$  deg [Fig. 5(b)], which could be attributed to the polarization characteristics of the SPP excitation. The propagation intensity of

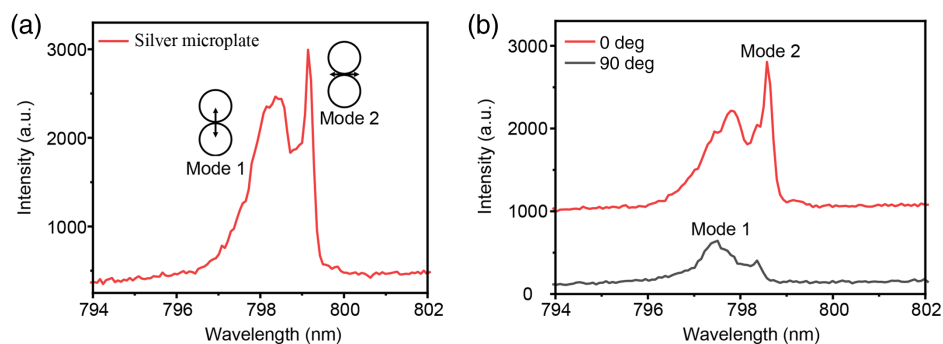


**Fig. 4** (a) Enlarged view of the lasing mode peak near 798 nm on the silver microplate. (b) Fluorescence spectrum of the corresponding lasing peak in panel (a) when the polarizer in the collected optical path was at 0 and 90 deg.

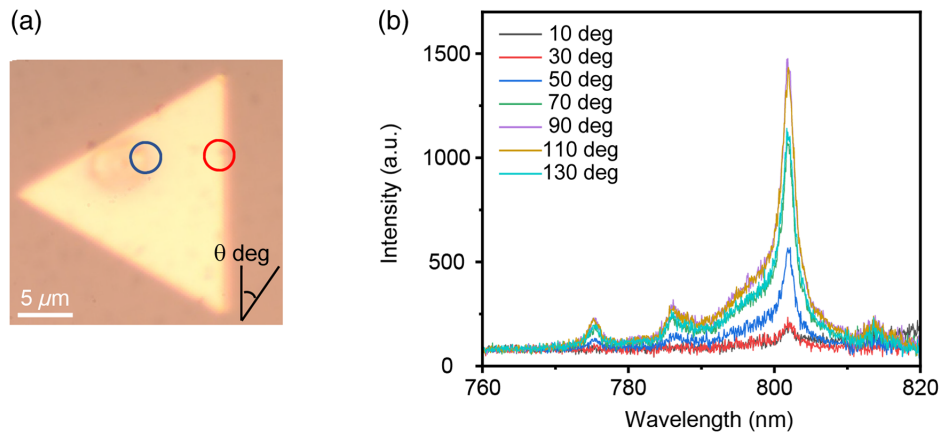


**Fig. 5** (a) Bright-field microscopy image of a microlaser remotely excited by SPPs. The red and blue circles represent the excitation and collection positions, respectively. The angle  $\theta$  in the lower right corner represents the polarization angle of the excited light. (b) Microcavity on the silver microplate at the excitation point corresponds to different emission spectra with the change in polarization angle of excitation light.

the SPPs is positively correlated with the vertical component of the electric vector,<sup>27</sup> with the SPP excitation exhibiting maximum strength when the excitation polarization is perpendicular to the edge of the silver microplate. This plasmon-assisted microlaser system enables investigations into mixed nonlinear nanophotonics and monomolecular remote-sensing applications.

### 3 Conclusion

In summary, we designed a simple and effective plasmon-assisted lanthanide-based microcavity that achieved TE polarization mode-selective enhancement and remote lasing excitation. Selective enhancement of the TE polarization mode was achieved through the introduction of local electromagnetic field amplification and the assistance of SPPs propagating on the surface of a silver microplate. Meanwhile, laser mode splitting was observed on the silver microplate owing to the coherent coupling between the microcavity and mirror microcavity modes. Moreover, because of the tens-of-micrometers long-distance propagation characteristics of SPPs on silver microplates, remote excitation and laser control were realized. These plasmon-assisted polarization-mode optional and remote-controllable upconversion microlasers hold significant potential in nonlinear hybrid nanophotonics, stochastic laser applications, and nano-optical sensing.

### Disclosures

The authors declare no competing financial interests.

### Code and Data Availability

The data supporting this letter are available from the corresponding authors upon reasonable request.

### Acknowledgments

This work was supported by the National Natural Science Foundation of China (Grant Nos. U22A6005, 92150110, 12074237, and 12304426), the National Key R&D Program of China (Grant Nos. 2020YFA0211300 and 2021YFA1201500), the Natural Science Foundation of Shaanxi Province (Grant

No. 2024JC-JCQN-07), the Fundamental Science Foundation of Shaanxi (Grant No. 22JSZ010), the Fundamental Research Funds for Central Universities (Grant Nos. GK202201012, GK202308001, and LHRCTS23065), and the Xi'an Young Elite Scientists Sponsorship Program (Grant No. 1203050367).

### References

1. F. Vollmer and S. Arnold, "Whispering-gallery-mode biosensing: label-free detection down to single molecules," *Nat. Methods*, **5**(7), 591–596 (2008).
2. Y. Zhi et al., "Single nanoparticle detection using optical microcavities," *Adv. Mater.* **29**(12), 1604920 (2017).
3. K. D. Heylman et al., "Optical microresonators for sensing and transduction: a materials perspective," *Adv. Mater.* **29**(30), 1700037 (2017).
4. T. J. Kippenberg et al., "Dissipative Kerr solitons in optical microresonators," *Science* **361**(6402), eaan8083 (2018).
5. T. J. Kippenberg, S. M. Spillane, and K. J. Vahala, "Kerr-nonlinearly optical parametric oscillation in an ultrahigh- $Q$  toroid microcavity," *Phys. Rev. Lett.* **93**(8), 083904 (2004).
6. X. Zhang et al., "Symmetry-breaking-induced nonlinear optics at a microcavity surface," *Nat. Photonics* **13**(1), 21–24 (2019).
7. Z. Shen et al., "Experimental realization of optomechanically induced non-reciprocity," *Nat. Photonics* **10**(10), 657–661 (2016).
8. M. Aspelmeyer, T. J. Kippenberg, and F. Marquardt, "Cavity optomechanics," *Rev. Mod. Phys.* **86**(4), 1391–1452 (2014).
9. L. Jin et al., "Enhancing multiphoton upconversion from NaYF<sub>4</sub>: Yb/Tm@NaYF<sub>4</sub> core-shell nanoparticles via the use of laser cavity," *ACS Nano* **11**(1), 843–849 (2017).
10. T. Wang et al., "White-light whispering-gallery-mode lasing from lanthanide-doped upconversion NaYF<sub>4</sub> hexagonal microrods," *ACS Photonics* **4**(6), 1539–1543 (2017).
11. X. Yang et al., "Lanthanide upconverted microlasing: microlasing spanning full visible spectrum to near-infrared under low power, CW pumping," *Small* **17**(41), 2103140 (2021).
12. Y. Liu et al., "Controlled assembly of upconverting nanoparticles for low-threshold microlasers and their imaging in scattering media," *ACS Nano* **14**(2), 1508–1519 (2020).
13. Y. Shang et al., "Low threshold lasing emissions from a single upconversion nanocrystal," *Nat. Commun.* **11**(1), 6156 (2020).
14. B. S. Moon et al., "Continuous-wave upconversion lasing with a sub-10 W cm<sup>-2</sup> threshold enabled by atomic disorder in the host matrix," *Nat. Commun.* **12**(1), 4437 (2021).

15. Q. Zhang et al., "Low threshold, single-mode laser based on individual CdS nanoribbons in dielectric DBR microcavity," *Nano Energy* **30**, 481–487 (2016).
16. B. Zhou et al., "Single-mode lasing and 3D confinement from perovskite micro-cubic cavity," *J. Mater. Chem. C* **6**(43), 11740–11748 (2018).
17. G. Wei et al., "Low-threshold organic lasers based on single-crystalline microribbons of aggregation-induced emission luminogens," *J. Phys. Chem. Lett.* **10**(3), 679–684 (2019).
18. L. Zhao et al., "High quality two-photon pumped whispering-gallery-mode lasing from ultrathin CdS microflakes," *J. Mater. Chem.* **7**(41), 12869–12875 (2019).
19. B. Tang et al., "Ultrahigh quality upconverted single-mode lasing in cesium lead bromide spherical microcavity," *Adv. Opt. Mater.* **6**(20), 1800391 (2018).
20. D. K. Gramotnev and S. I. Bozhevolnyi, "Plasmonics beyond the diffraction limit," *Nat. Photonics* **4**, 83–91 (2010).
21. D. Dai, J. Bauters, and J. E. Bowers, "Passive technologies for future large-scale photonic integrated circuits on silicon: polarization handling, light non-reciprocity and loss reduction," *Light: Sci. Appl.* **6**, e1 (2012).
22. J. Chee, S. Zhu, and G. Q. Lo, "CMOS compatible polarization splitter using hybrid plasmonic waveguide," *Opt. Express* **20**(23), 25345–25355 (2012).
23. Z. Wu and Z. Xu, "Achromatic on-chip focusing of graphene plasmons for spatial inversions of broadband digital optical signals," *Adv. Photonics Nexus* **2**(5), 056003 (2023).
24. M. Jung and G. Shvets, "Emergence of tunable intersubband-plasmon-polaritons in graphene superlattices," *Adv. Photonics* **5**(2), 026004 (2023).
25. H. Dong et al., "Versatile spectral and lifetime multiplexing nano-platform with excitation orthogonalized upconversion luminescence," *ACS Nano* **11**(3), 3289–3297 (2017).
26. H. Dong et al., "Selective cation exchange enabled growth of lanthanide core/shell nanoparticles with dissimilar structure," *J. Am. Chem. Soc.* **139**(51), 18492–18495 (2017).
27. T. Zhang et al., "Controlled multichannel surface plasmon polaritons transmission on atomic smooth silver triangular waveguide," *Adv. Opt. Mater.* **7**(21), 1900930 (2019).
28. H. Chen et al., "Multiplasmons-pumped excited-state absorption and energy transfer upconversion of rare-earth-doped luminescence beyond the diffraction limit," *ACS Photonics* **8**(5), 1335–1343 (2019).
29. H. Chen et al., "Sub-50-ns ultrafast upconversion luminescence of a rare-earth-doped nanoparticle," *Nat. Photonics* **16**(9), 651–657 (2022).
30. A. B. Vasista et al., "Vectorial fluorescence emission from microsphere coupled to gold mirror," *Adv. Opt. Mater.* **6**(22), 1801025 (2018).